Geometric-Phase Interference in a Mn**12** Single-Molecule Magnet with Fourfold Rotational Symmetry

S. T. Adams,[1] E. H. da Silva Neto,[1,*] S. Datta,[1] J. F. Ware,[1,†] C. Lampropoulos,[2,‡] G. Christou,[2] Y. Myaesoedov,[3] E. Zeldov,[3] and Jonathan R. Friedman[1,4,§]

[1]*Department of Physics, Amherst College, Amherst, Massachusetts 01002-5000, USA*
[2]*Department of Chemistry, University of Florida, Gainesville, Florida 32611, USA*
[3]*Department of Condensed Matter Physics, The Weizmann Institute of Science, Rehovot 76100, Israel*
[4]*Institute for Quantum Computing, University of Waterloo, Waterloo, Ontario, Canada N2L 3G1*
(Received 22 October 2012; revised manuscript received 11 January 2013; published 20 February 2013)

We study the magnetic relaxation rate Γ of the single-molecule magnet Mn$_{12}$-tBuAc as a function of the magnetic field component H_T transverse to the molecule's easy axis. When the spin is near a magnetic quantum tunneling resonance, we find that Γ increases abruptly at certain values of H_T. These increases are observed just beyond values of H_T at which a geometric-phase interference effect suppresses tunneling between two excited energy levels. The effect is washed out by rotating H_T away from the spin's hard axis, thereby suppressing the interference effect. Detailed numerical calculations of Γ using the known spin Hamiltonian accurately reproduce the observed behavior. These results are the first experimental evidence for geometric-phase interference in a single-molecule magnet with true fourfold symmetry.

Geometric-phase effects are responsible for many fascinating phenomena in classical and quantum physics from how a cat rights itself while in free fall to the dynamics of charged particles in electromagnetic fields, e.g., the Aharonov-Bohm effect [1]. One formulation of geometric-phase effects involves a path-integral approach in which the interference of paths is modulated by the geometric phase difference between the paths [2–5]. Such interference effects can reveal the underlying symmetries of the system's Hamiltonian. The dynamics of spins provide a natural way to explore quantum geometric phases for, as Berry showed in his pioneering work [6], a system near a degeneracy point can be mapped onto a spin in an effective magnetic field.

Single-molecule magnets (SMMs) are an ideal test bed for exploring spin geometric-phase interference. In these systems, each molecule behaves as a large spin with a well-defined Hamiltonian determined by the symmetry of the molecule and its environment [7]. The interactions between molecules in a crystal are typically weak and the sample behaves as an ensemble of nominally identical large-spin objects. In many SMMs, the spins have a large anisotropy barrier separating the preferred "up" and "down" directions. This leads to hysteresis and slow relaxation between these easy-axis directions. A geometric-phase effect can lead to interference between tunneling paths, thus modulating the rate at which spins flip direction. In a ground-breaking experiment, Wernsdorfer and Sessoli [8] found oscillations in the probability of magnetization tunneling as a field applied along the hard axis modulated the interference between two tunneling paths. This observation confirmed a theoretical prediction by Garg [4] and ignited intense theoretical study of related phenomena [9–17]. Geometric-phase interference between

tunneling paths has been observed in other SMMs that have effective twofold symmetry, where tunneling involves the interference between two equal-amplitude paths [18]. It has also been seen in antiferromagnetic molecular wheels [19] and in SMM dimers [20,21]. Such interference effects in the bellwether SMM Mn$_{12}$Ac are complicated by the presence of solvent disorder [22], which breaks the SMM's nominal fourfold symmetry, resulting in a competition between second-order and fourth-order anisotropies [23,24]. Here we report the observation of a geometric-phase interference effect in [Mn$_{12}$O$_{12}$(O$_2$CCH$_2$-^{t}Bu)$_{16}$(CH$_3$OH)$_4$] $\cdot$ CH$_3$OH (hereafter Mn$_{12}$-tBuAc), a variant of Mn$_{12}$Ac that is free of solvent disorder and maintains its fourfold rotational symmetry [25–29]. Unlike previous observations of geometric-phase interference, which involved ground-state tunneling, the interference effect described herein is observed in the thermally assisted tunneling regime where tunneling takes place near the top of the barrier. The interference effect provides a fingerprint that affords an unprecedented ability to clearly identify which levels participate in the thermally assisted process.

In 2002, Park and Garg [30] and, independently, Kim [31], predicted that an interference effect should be observed in SMMs with fourth-order transverse anisotropy, described by the Hamiltonian

$$\mathcal{H} = -DS_z^2 + (C/2)(S_+^4 + S_-^4) - g\mu_B S \cdot H, \quad (1)$$

where $S_\pm = S_x \pm iS_y$. In zero field, such a spin system has the classical energy landscape shown in the left inset of Fig. 1. Applying a magnetic field H_T along one of the four hard directions ($\pm x$ and $\pm y$ for $C > 0$) preserves reflection symmetry through the z-hard plane, allowing interference between equal-amplitude tunneling paths
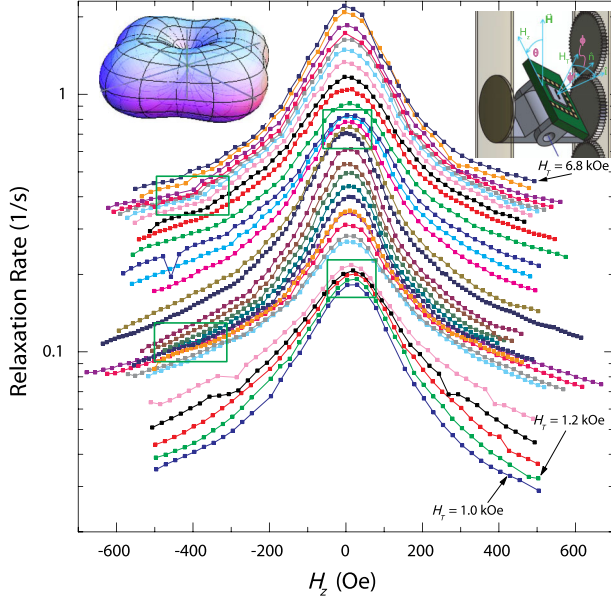
FIG. 1 (color online). Measured magnetic relaxation rate as a function of longitudinal field near the zero-field resonance for several values of transverse field (H_T) from 1.0 to 6.8 kOe in 200 Oe increments. The data were taken from sample A at 3.10 K. The green boxes indicate regions where curves for different values of H_T tend to bunch together. The left inset shows the classical energy landscape in a spherical polar plot for a spin described by Eq. (1). The z axis is the easy axis (energy minima) while the x and y axes are the hard axes (maxima). The value of C has been greatly exaggerated to make the fourfold symmetry evident. The right inset shows a schematic of the apparatus, illustrating control of angles θ and ϕ. $\hat{\mathbf{n}}$ is normal to detector plane; $\hat{\mathbf{i}}$ is a hard axis direction.

that virtually pass through the saddle points in the landscape. This interference induces oscillations in the tunneling probability as a function of H_T. Mn$_{12}$-tBuAc is reasonably well described by the above Hamiltonian with the addition of sixth-order terms consistent with fourfold symmetry [27]:

$$\mathcal{H} = -DS_z^2 - AS_z^4 - A'S_z^6 + (C/2)(S_+^4 + S_-^4)$$
$$+ (C'/2)[S_z^2(S_+^4 + S_-^4) + \text{H.c.}]$$
$$- \mu_B[g_z S_z H_z + g_\perp(S_x \cos\phi + S_y \sin\phi)H_T], \quad (2)$$

where $D = 0.568$ K, $A = 0.69$ mK, $A' = 3.3$ μK, $C = 50$ μK, $C' = -0.79$ μK, $g_z = 2.00$, and $g_\perp = 1.93$. H_z is the longitudinal component of the magnetic field, and ϕ measures the angle between H_T and the x axis. Much of the system's dynamics can be understood in terms of the double-well potential shown in the inset of Fig. 2(a), which shows the system's energy as a function of the angle between the spin vector and the easy axis (z) direction. The spin has $2S + 1$ energy levels, which are approximate eigenstates of S_z. H_z tilts the potential and at certain values, levels in opposite wells align, allowing resonant tunneling between wells that results in a marked increase in the magnetic relaxation rate. The fourth and fifth terms in Eq. (2) as well as H_T break the commutation of $\mathcal{H}$
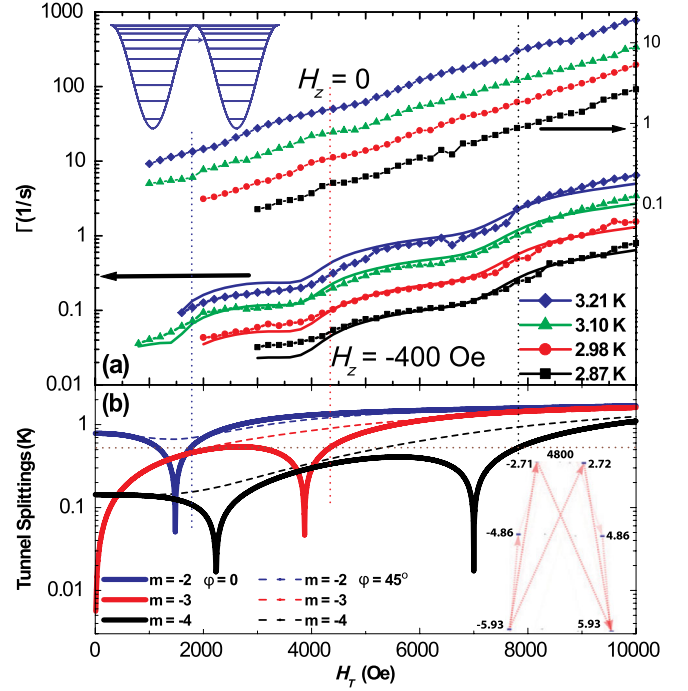

FIG. 2 (color online). (a) Relaxation rate as a function of transverse field at $H_z = 0$ and $H_z = -400$ Oe, taken from the data shown in Fig. 1. The solid curves are the results of simulations of the relaxation rate using Eq. (2) with $\phi = 7°$, as described in the text. The inset shows the double-well potential for the $n = 0$ tunneling resonance. (b) Calculated tunnel splitting for energy-level pairs $m = \pm 2$, $m = \pm 3$, and $m = \pm 4$, as indicated, for $\phi = 0$ (solid lines) and $\phi = 45°$ (dashed lines). The dotted horizontal line marks a threshold splitting at which the system makes a transition from one dominant pair of tunneling levels to another. The dotted vertical lines show the transverse field at which this transition occurs and its correspondence to the observed rapid increases in the relaxation rate. Inset: Probability current diagram for high-lying energy levels at $H_T = 4.8$ kOe. The numerical labels indicate the expectation values of S_z for the corresponding energy level; the opacity of the arrows indicates the magnitude of the associated current.

and S_z, thereby inducing tunneling. The tunnel splitting between nearly degenerate states is readily calculated by diagonalizing Eq. (2). The solid lines in Fig. 2(b), for $\phi = 0$ (mod 90°), show that destructive interference between tunneling paths induces a dramatic suppression ("quenching") of tunneling at discrete values of H_T for each pair of levels [32]. (Here and below, we label each state by m, its value of $\langle S_z \rangle$ in the absence of tunneling.) The interference effect is largely destroyed when ϕ is increased towards 45° (dashed lines) since H_T then favors one tunneling path over others. The tunneling quenching affects which levels are involved in the magnetic relaxation process, as evidenced by our data.

Crystals of Mn$_{12}$-tBuAc were synthesized according to published procedures [29]. A sample was mounted adjacent to a Hall sensor that was in turn mounted on a rotator probe. A reference sensor on the same chip was used to measure background signals. Signals from the two

sensors were subtracted with an analog circuit. We performed extensive measurements on two samples (A and B). Measurements of sample B were performed using a modified apparatus (Fig. 1 right inset) in which the orientation of both the sample's easy and hard axes relative to the field could be adjusted (the latter *ex situ* by $\sim \pm 35°$). Measurements were performed as follows. The sample was rotated to align its easy axis with the external magnetic field, magnetizing the sample, i.e., populating one of the wells in the inset of Fig. 2(a). Next, the sample was rotated to an orientation that produced the desired values of H_z and H_T. The subsequent time dependence of the magnetization was monitored and fit to an exponential decay to extract the relaxation rate, Γ. Proceeding this way, we obtained values for Γ as a function of H_z and H_T and of temperature T for relaxation near a tunneling resonance.

Some data from sample A are shown in Fig. 1, where Γ is plotted as a function of H_z for several values of H_T at $T = 3.10$ K. For each value of H_T, Γ exhibits a roughly Lorentzian dependence on H_z, peaked at $H_z = 0$, where tunneling is maximum. Γ generally increases with increasing H_T as the tunneling rate is enhanced and, in tandem, the effective energy barrier is reduced [33]. We note that for some regions of H_T and H_z (green boxes) the data are bunched—the relaxation rate changes very little with increasing H_T. The effect is much more pronounced in the shoulders of the peak than near its center. Figure 2 shows Γ as a function of H_T for $H_z = 0$ (upper four data sets, from peak center in Fig. 1) and $H_z = -400$ Oe (lower four data sets, from peak shoulders). All sets show a roughly exponential increase in Γ with H_T. In addition, Γ exhibits steps and plateaus (the latter corresponding to the bunching in Fig. 1). These are far more apparent in the $H_z = -400$ Oe data. Each step corresponds to a transition from one dominant pair of tunneling levels (e.g., $m = \pm 3$) to another (e.g., $m = \pm 4$). Interestingly, theoretical calculations of these transitions for $C = C' = 0$ predict that the transitions should be independent of ϕ and more pronounced on resonance ($H_z = 0$) than away from resonance [34,35], in contrast to our results. Structure near $H_z = 0$, where Γ depends strongly on H_z, may be washed out by inhomogeneous dipole fields. More importantly, the structure observed near $H_z = -400$ Oe (where Γ is less sensitive to dipole fields) is much more pronounced than predicted by the simple model. Including the experimentally determined values of C and C' in Eq. (2) induces the tunneling suppression shown in Fig. 2(b). These tunnel quenches, in turn, give rise to the steps in Γ.

To illustrate this, Fig. 2(b) contains a horizontal dotted line—an empirically determined "tunnel threshold." When the tunnel splitting for a particular pair of levels approaches this threshold, tunneling for that pair begins to become the dominant relaxation mechanism [33,34,36,37]. For example, at $H_T \sim 4.2$ kOe (marked by the red vertical dotted line), the tunnel splitting for $m = \pm 3$ reaches the threshold and tunneling between these levels begins to dominate over relaxation through higher levels. This additional relaxation mechanism produces the rapid increase in Γ near this field.

Similar transitions occur when other pairs of levels reach the threshold, marked by the other dotted vertical lines in the figure. The tunneling suppression effect plays a crucial role here: it determines how rapidly the threshold is crossed as H_T increases. The slope of the tunnel splittings curves in Fig. 2(b) is rather steep in the vicinity of the threshold right after a quench for $\phi = 0$. In contrast, when $\phi = 45°$, the tunnel splitting quenches are absent and the tunnel splittings cross the threshold more gradually, making each transition so broad that it overlaps with others so that its observability is washed out.

This effect is demonstrated in Fig. 3. The inset of the figure shows Γ as a function of H_T for sample B in the vicinity of one of the transitions for several values of $\phi' = \phi + \phi_0$, where ϕ' is the experimental azimuthal angle of the rotator's second stage and ϕ_0 is a constant offset representing the orientation of the sample's hard axis (see Fig. 1 right inset). The data features for sample B were less distinct than for sample A, possibly because B was measured more than a year after synthesis. To enhance clarity, we divided the data by $e^{0.3 H_T / \text{kOe}}$, where the coefficient 0.3 was chosen empirically. The resulting data are presented in the main figure. For $\phi' = 2°$ and $20°$, the sharp transition at ~ 8 kOe is apparent while it is clearly suppressed for values of ϕ' outside this range. These results suggest $\phi_0 \sim 9°$, implying that the hard axes for the $m = 2$–4 levels are roughly parallel with the a and b crystallographic axes of the cuboid-shaped crystals [38].

We also studied the relaxation rate near the $n = 1$ ($H_z \sim 4.5$ kOe) resonance. We examined sample B with $\phi' = 2°$ with $H_z \sim 1$ kOe below the resonance peak. Again we see steps in the relaxation rate as a function of H_T, as shown in Fig. 4(a). (Like in Fig. 3, we have removed an exponential background for clarity.) The steps here also correspond to the transitions between dominant tunneling
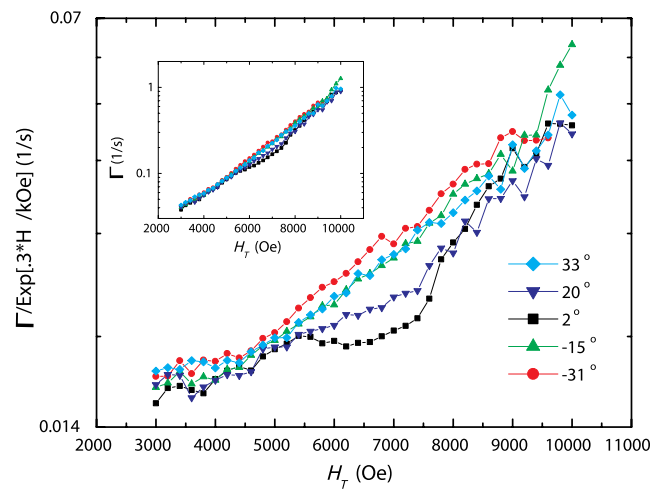
FIG. 3 (color online). Relaxation rate from sample B as a function of transverse field for several different values of ϕ' for $H_z = -500$ Oe. The inset shows the raw relaxation rate while the main figure shows the same data after dividing by an exponential function to enhance clarity.
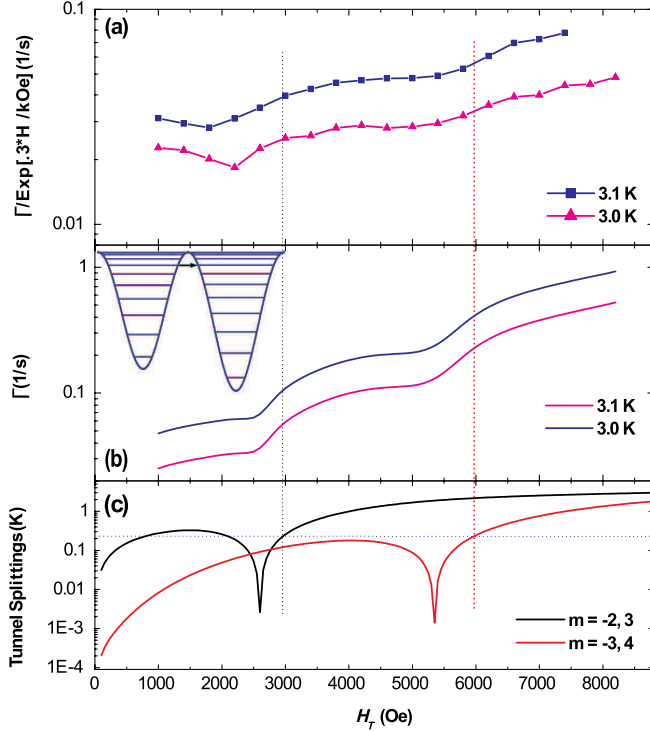
FIG. 4 (color online).　(a) Relaxation rate (after dividing by an exponential to enhance presentation) as a function of H_T for H_z near the $n = 1$ resonance. Data was taken from sample B with experimental azimuthal angle $\phi' = 2°$ and H_z set to 1 kOe less than the peak of the resonance. (b) Simulations of relaxation rate as a function of transverse field using Eqs. (2)–(4) with $\phi = 7°$. The inset shows the double-well potential for the $n = 1$ resonance. (c) Tunnel splitting calculations with $\phi = 0°$ for the $m = -2, 3$ and $m = -3, 4$ energy-level pairs, as indicated. The dotted horizontal line represents a tunneling threshold while the dotted vertical lines correspond to the transverse fields at which abrupt transitions in relaxation rate occur.

level pairs, as illustrated in Fig. 4(c), each occurring when the tunnel splitting for a particular pair rapidly crosses a threshold value (horizontal dotted line) in the wake of a quench.

We performed numerical calculations of Γ using a master equation approach [34,35,37,39–41] to treat spin-phonon interactions. For calculational ease, we used the spin's energy eigenbasis, which incorporates tunneling effects automatically since the eigenstates of Eq. (2) are superpositions of S_z eigenstates. We neglect off-diagonal elements in the density matrix, a good approximation since our experiments were done away from the exact resonance conditions where such elements are appreciable. The master equation governing the population of each level, p_i, is

$$\frac{dp_i}{dt} = \sum_{\substack{j=1 \\ i \neq j}}^{21} -(\gamma_{ij}^{(1)} + \gamma_{ij}^{(2)})p_i + (\gamma_{ji}^{(1)} + \gamma_{ji}^{(2)})p_j. \quad (3)$$

The phonon transition rates are given by [34,42]

$$\gamma_{ij}^{(\alpha)} = \frac{\kappa^{(\alpha)} D^2}{6\pi\rho c_s^5 \hbar^4} |s_{ij}^{(\alpha)}|^2 \Delta_{ij}^3 N(\Delta_{ij}), \quad (4)$$

where $s_{ij}^{(1)} = \langle i|\{S_x, S_z\}|j\rangle$ and $s_{ij}^{(2)} = \langle i|S_x^2 - S_y^2|j\rangle$ and $\Delta_{ij} = \varepsilon_i - \varepsilon_j$, with ε_i the energy of level $|i\rangle$. $N(\Delta) = (e^{\Delta/k_B T} - 1)^{-1}$ is the phonon thermal distribution function, $\rho = 1.356 \times 10^3$ kg/m³ is the mass density [27], and c_s is the transverse speed of sound. $\kappa^{(1)} = 1$ and $\kappa^{(2)}$ is a constant of order unity representing the strength of the associated spin-phonon coupling mechanism [43]. We neglect possible collective spin-phonon interactions [46].

We calculated Γ by finding the slowest nonzero eigenvalue of the rate matrix implicit in Eq. (3). The calculated rates are fit to the data in Fig. 2, allowing c_s, $\kappa^{(2)}$, C, and C' to be unconstrained parameters. The remaining Hamiltonian parameters were fixed and we set $H_z = -400$ Oe and $\phi = 7°$. The results of the fitting are shown by the solid curves in Fig. 2(a). The calculated rates reproduce the data quite well. The fit yields $c_s = 1122$ m/s and $\kappa^{(2)} = 1.21$. These parameters set the overall scale of the rate and the general slope of the rate versus H_T, respectively. They do not influence the positions of the steps, which are determined by Hamiltonian parameters C and C'. The fit yields $C = 55$ μK and $C' = -0.81$ μK, in good agreement with the values determined spectroscopically [27]. Using the same parameters, we can also calculate Γ for the $n = 1$ resonance, shown in Fig. 4(b). Again, the calculations accurately reproduce the structure of the measured relaxation rates. [Because of the large background for the sample B data (Figs. 3 and 4), fits of that data do not produce physically meaningful values of c_s and $\kappa^{(2)}$.]

Our calculations allow us to precisely determine which pairs of levels dominate the tunneling process as a function of H_T. The inset of Fig. 2(b) shows an example of the probability "currents" (dashed arrows) [37] between some of the relevant states at $H_T = 4.8$ kOe. The state labels indicate the values of $\langle S_z \rangle$. Diagonal arrows correspond to tunneling transitions in the energy eigenbasis—such transitions would be forbidden in the absence of tunneling. For this example, $m = \pm 3$ are clearly the dominant tunneling levels. These calculations confirm the interpretation of the steps in the relaxation rate given above, e.g., for $n = 0$ at $H_T \sim 4.2$ kOe the dominant tunneling pair switches from $m = \pm 2$ to $m = \pm 3$.

In conclusion, our measurements provide the first evidence for a geometric-phase interference effect in a truly fourfold symmetric SMM. The results also demonstrate this effect in the thermally assisted tunneling regime, allowing identification of which levels dominate the tunneling process. It may be possible to observe similar effects in this system in ground-state tunneling. Such experiments would require lower temperatures and higher magnetic fields.

---

*Present address: Department of Physics, Princeton University, Jadwin Hall, Princeton, NJ 08544, USA.
†Present address: Department of Physics, University of Michigan, 450 Church Street, Ann Arbor, MI 48109-1040, USA.
‡Present address: University of North Florida, Department of Chemistry, Building 50, Room 3500, 1 UNF Drive, Jacksonville, FL 32224-7699, USA.
§Corresponding author.
jrfriedman@amherst.edu

[1] A. Shapere and F. Wilczek, *Geometric Phases in Physics*, Advanced Series in Mathematical Physics, Vol. 5 (World Scientific, Singapore, 1989), p. 528.

[2] D. Loss, D. P. DiVincenzo, and G. Grinstein, Phys. Rev. Lett. **69**, 3232 (1992).

[3] J. von Delft and C. L. Henley, Phys. Rev. Lett. **69**, 3236 (1992).

[4] A. Garg, Europhys. Lett. **22**, 205 (1993).

[5] J. R. Friedman and D. V. Averin, Phys. Rev. Lett. **88**, 050403 (2002).

[6] M. V. Berry, Proc. R. Soc. A **392**, 45 (1984).

[7] J. R. Friedman and M. P. Sarachik, Annu. Rev. Condens. Matter Phys. **1**, 109 (2010).

[8] W. Wernsdorfer and R. Sessoli, Science **284**, 133 (1999).

[9] A. Garg, Europhys. Lett. **50**, 382 (2000); Phys. Rev. B **64**, 094413 (2001); **64**, 094414 (2001).

[10] G. H. Kim, Phys. Rev. B **60**, R3728 (1999).

[11] E. M. Chudnovsky and X. Martinez-Hidalgo, Europhys. Lett. **50**, 395 (2000).

[12] R. Lu, H. Hu, J. L. Zhu, X. B. Wang, L. Chang, and B. L. Gu, Phys. Rev. B **61**, 14581 (2000).

[13] E. Kececioglu and A. Garg, Phys. Rev. B **63**, 064422 (2001); Phys. Rev. Lett. **88**, 237205 (2002).

[14] Z.-D. Chen, Europhys. Lett. **62**, 726 (2003).

[15] P. Bruno, Phys. Rev. Lett. **96**, 117208 (2006).

[16] M. N. Leuenberger and E. R. Mucciolo, Phys. Rev. Lett. **97**, 126601 (2006).

[17] M. S. Foss-Feig and J. R. Friedman, Europhys. Lett. **86**, 27 002 (2009).

[18] W. Wernsdorfer, S. Bhaduri, C. Boskovic, G. Christou, and D. N. Hendrickson, Phys. Rev. B **65**, 180403(R) (2002); W. Wernsdorfer, N. E. Chakov, and G. Christou, Phys. Rev. Lett. **95**, 037203 (2005).

[19] O. Waldmann, T. C. Stamatatos, G. Christou, H. U. Güdel, I. Sheikin, and H. Mutka, Phys. Rev. Lett. **102**, 157202 (2009).

[20] C. M. Ramsey, E. del Barco, S. Hill, S. J. Shah, C. C. Beedle, and D. N. Hendrickson, Nat. Phys. **4**, 277 (2008).

[21] W. Wernsdorfer, T. C. Stamatatos, and G. Christou, Phys. Rev. Lett. **101**, 237204 (2008).

[22] A. Cornia, R. Sessoli, L. Sorace, D. Gatteschi, A. L. Barra, and C. Daiguebonne, Phys. Rev. Lett. **89**, 257201 (2002).

[23] E. del Barco, A. D. Kent, E. M. Rumberger, D. N. Hendrickson, and G. Christou, Phys. Rev. Lett. **91**, 047203 (2003).

[24] E. del Barco, A. D. Kent, S. Hill, J. M. North, N. S. Dalal, E. M. Rumberger, D. N. Hendrickson, N. Chakov, and G. Christou, J. Low Temp. Phys. **140**, 119 (2005).

[25] S. Hill, N. Anderson, A. Wilson, S. Takahashi, N. E. Chakov, M. Murugesu, J. M. North, N. S. Dalal, and G. Christou, J. Appl. Phys. **97**, 10M510 (2005); S. Hill, N. Anderson, A. Wilson, S. Takahashi, K. Petukhov, N. E. Chakov, M. Murugesu, J. M. North, E. del Barco, A. D. Kent, N. S. Dalal, and G. Christou, Polyhedron **24**, 2284 (2005).

[26] M. Soler, P. Artus, K. Folting, J. C. Huffman, D. N. Hendrickson, and G. Christou, Inorg. Chem. **40**, 4902 (2001).

[27] A.-L. Barra, A. Caneschi, A. Cornia, D. Gatteschi, L. Gorini, L.-P. Heiniger, R. Sessoli, and L. Sorace, J. Am. Chem. Soc. **129**, 10 754 (2007).

[28] E. Burzurí, C. Carbonera, F. Luis, D. Ruiz-Molina, C. Lampropoulos, and G. Christou, Phys. Rev. B **80**, 224428 (2009).

[29] C. Lampropoulos, M. Murugesu, A. G. Harter, W. Wernsdorfer, S. Hill, N. S. Dalal, A. P. Reyes, P. L. Kuhns, K. A. Abboud, and G. Christou, Inorg. Chem. **52**, 258 (2013).

[30] C.-S. Park and A. Garg, Phys. Rev. B **65**, 064411 (2002).

[31] G.-H. Kim, J. Appl. Phys. **91**, 3289 (2002).

[32] Our calculated tunnel splittings differ somewhat from those presented in Ref. [27], even when we use the same Hamiltonian parameters as those reported in that paper.

[33] J. R. Friedman, Phys. Rev. B **57**, 10291 (1998).

[34] D. A. Garanin and E. M. Chudnovsky, Phys. Rev. B **56**, 11102 (1997).

[35] D. A. Garanin, in *Advances in Chemical Physics* (John Wiley & Sons, Inc., Hoboken, NJ, 2011), Vol. 147, pp. 213–277.

[36] J. R. Friedman, in *Exploring the Quantum/Classical Frontier: Recent Advances in Macroscopic Quantum Phenomena*, edited by J. R. Friedman and S. Han (Nova Science, Hauppauge, NY, 2003), pp. 179–218.

[37] M. N. Leuenberger and D. Loss, Phys. Rev. B **61**, 1286 (2000).

[38] In contrast, Ref. [27] reports that the hard axes are ~45° from the a and b axes. This apparent discrepancy arises because C and C' have opposite signs, causing the hard-axis directions to depend on which levels m are probed.

[39] J. Villain, F. Hartmann-Boutron, R. Sessoli, and A. Rettori, Europhys. Lett. **27**, 159 (1994).

[40] F. Luis, J. Bartolomé, and J. F. Fernández, Phys. Rev. B **57**, 505 (1998).

[41] A. Fort, A. Rettori, J. Villain, D. Gatteschi, and R. Sessoli, Phys. Rev. Lett. **80**, 612 (1998).

[42] M. N. Leuenberger and D. Loss, Europhys. Lett. **46**, 692 (1999).

[43] There has been some debate about the magnitude and even the existence of $\gamma_{ij}^{(2)}$ [44,45]. However, we find including it necessary to get a reasonable fit to our data.

[44] E. M. Chudnovsky and D. A. Garanin, Europhys. Lett. **52**, 245 (2000).

[45] M. N. Leuenberger and D. Loss, Europhys. Lett. **52**, 247 (2000).

[46] C. Calero, E. M. Chudnovsky, and D. A. Garanin, Phys. Rev. B **76**, 094419 (2007).